μSR and neutron diffraction studies on the tuning of spin-glass phases in the partially ordered double perovskites $SrMn_{1-x}W_xO_3$

Poonam Yadav,[1] Shivani Sharma,[2] Peter J. Baker,[2] Pabitra K. Biswas,[2] Ivan da Silva,[2] Rajamani Raghunathan,[1] Uday Deshpande,[1] R. J. Choudhary,[1] N. P. Lalla,[1,*] and A. Banerjee[1]

[1]*UGC-DAE Consortium for Scientific Research, Indore-452001, India*

[2]*ISIS Facility, Rutherford Appleton Laboratory, Chilton, Didcot OX11 0QX, United Kingdom*

(Received 17 April 2018; revised manuscript received 26 April 2019; published 14 June 2019)

We have studied the partially ordered double perovskite (PODP) and spin-glass phase in $Sr(Mn_{1-x}W_x)O_3$ ($x = 0.20$ to 0.40) using neutron powder diffraction (NPD), muon spin relaxation (μSR), magnetic susceptibility (χ), and x-ray photoelectron spectroscopy measurements. Structural studies reveal that $SrMn_{1-x}W_xO_3$ undergoes a quasicontinuous transformation from simple perovskite (Pm-3m) to PODP ($P2_1/n$) phase as x increases. $\chi_{dc}(T)$ and $\chi_{ac}(T)$ measurements show a sharp cusplike peak at spin-glass transition T_g. The muon relaxation rate (λ) peaks at T_g following a critical growth, given by $\lambda = \lambda(0)\tau^{-w}[\tau = (T-T_g)/T_g]$. No long-range magnetic order is observed in NPD below T_g. These measurements confirm a tunable spin-glass state of $SrMn_{1-x}W_xO_3$ for $0.2 < x < 0.4$. The spin-glass phase appears with the onset of Mn^{2+} cations, which induce competing ferro-antiferro interactions leading to exchange frustration. The T_g decreases as the W content and Mn^{2+} concentration increase. Our results suggest that the spin-glass phase can be tuned through the relative concentration of 2+, 3+, and 4+ Mn ions.

DOI: 10.1103/PhysRevB.99.214421

I. INTRODUCTION

The occurrence of exotic magnetic ground states like spin liquid [1–5], valence bond glass [6], spin glass [7–11], and spin ice [12,13] have been of immense theoretical and experimental interest for several decades [14–17]. These exotic magnetic phases originate from magnetic frustration arising from competing nearest neighbor (NN) and next nearest neighbor (NNN) antiferromagnetic (AFM) interactions between moments arranged on triangular, tetrahedral [18], kagome [19], and Shastry-Sutherland [20] type lattices. Due to the presence of tetrahedral topology in their structure, as shown in the inset of Fig. 1(a), magnetic double perovskites (DPs) of the general chemical formula [6,21–23] $A_2BB'O_6$ have been extensively studied regarding such exotic magnetic ground states. In magnetic DPs [24] B/B' (diamagnetic/magnetic) cations follow a tetrahedral topology; therefore an AFM superexchange interaction cannot be simultaneously satisfied at each lattice site, and hence long-range AFM order is suppressed. Such an interaction gives rise to cooperative phenomena resulting in frustration-driven freezing of spin configurations, such as valence bond glass Ba_2YMoO_6 [6] and spin glass as in Sr_2CaReO_6 [21], Ba_2YReO_6 [22], and Sr_2MgReO_6 [23]. However, there are examples, where despite the presence of tetrahedral topology, magnetic DPs undergo normal AFM ordering [25,26].

An ideal DP has Fm-3m structure, but it is often distorted due to steric pressure and temperature variations [27,28] resulting in its structural variants like $P4_2/n$, $Pnma$, $P2_1/m$, $P2_1/n$, etc. The B-site chemical ordering of B/B' cations still exists [28–30], but the tetrahedral topology can be distorted relaxing the condition of frustration and resulting in AFM ordering. In such DPs the NN AFM interaction is an extended superexchange, active along B'-O-B-O-B' pathways and leads to type-I AFM, e.g., Ca_2LaRuO_6 [31], Sr_2YRuO_6 [32], Sr_2LuRuO_6, Ba_2YRuO_6, Ba_2LuRuO_6 [33], La_2LiRuO_6 [34], and Sr_2TeMnO_6 [35]. It has been shown that DPs having diamagnetic atoms like W [25,26,36,37], Nb [38], or Mo [26], at their B sites exhibit type-II AFM in which the NNN spins are AFM aligned.

It is worth noting that in the case of perovskites the frustrated magnetic ground states have been studied mostly on perfectly ordered DPs. No attempts have been made to study the evolution of magnetic frustration as a function of B-site substitution. The flexibility of the perovskite structures for B-site substitution provides a unique opportunity for such studies. For DP structures it is not yet known, under the favorable conditions of ionic size and charge states of B/B', what minimum substitution can result in the formation of $A_2B'_{2-x}B_xO_6$ type partially ordered double perovskites (PODPs) or whether a PODP even forms. The physical properties of perovskites are mostly governed by the BO_6 octahedra so a quasicontinuous variation of B-site occupancies in PODPs can provide tunability of their physical properties. The coexistence of various charge states of B' probably arising due to substitution of B, and B'-O-B' and B'-O-B-O-B', mixed superexchange pathways in a PODP should alter the magnetic interactions and result in frustrated spin lattices with exotic magnetic phases.

To address these questions we have carried out studies on distorted DPs with compositions typified by $A(B'_{1-x}B_x)O_3$ taking $Sr(Mn_{1-x}W_x)O_3$ as a case study, with x ranging from 0.2 to 0.4. The end members of $Sr(Mn_{1-x}W_x)O_3$, i.e.,

*nplallaiuc82@gmail.com

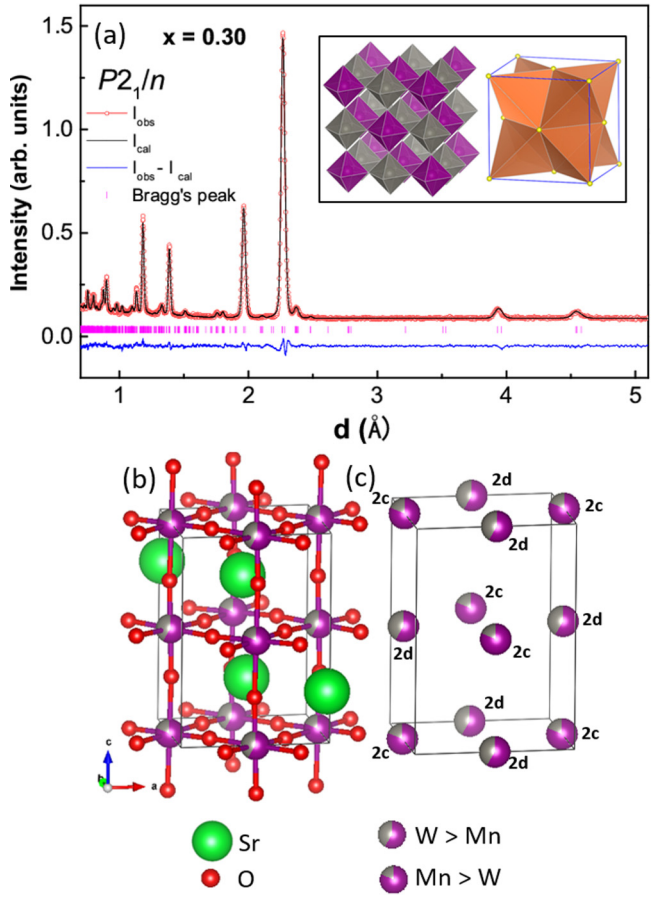

FIG. 1. (a) Rietveld refined time-of-flight (TOF) neutron powder diffraction profile of $Sr(Mn_{1-x}W_x)O_3$ for $x = 0.30$. Inset shows the structure of a double perovskite phase, highlighting the presence of tetrahedral topology of B/B' cations. (b) A typical crystal structure model of a partially ordered double perovskite of $Sr(Mn_{1-x}W_x)O_3$ obtained after Rietveld refinement. (c) It depicts the biased occupancies of Mn at $2c$ and W at $2d$ sites for $x = 0.30$. Atoms have been indicated in different colors.

$SrMnO_3$ ($x = 0$), space group $Pm\text{-}3m$ [39], and the perfectly ordered DP $SrMn_{0.5}W_{0.5}O_3$ or equivalently $Sr_2(MnW)O_6$, space-group $P2_1/n$ [26], both order antiferromagnetically along superexchange pathways Mn-O-Mn and Mn-O-W-O-Mn at their Néel transition temperatures $(T_N) = 260$ and 13.6 K, respectively. $SrMnO_3$ is reported to order as G type with propagation vector (1/2, 1/2, 1/2) [39] and $Sr_2(MnW)O_6$ is reported to order as AFM with propagation vector (1/2,0,1/2) [26]. We have found that $Sr(Mn_{1-x}W_x)\,O_3$ forms PODPs for $x \geqslant 0.3$, while the compositions with $x < 0.3$ remain simple disordered perovskites. The magnetic and structural properties of PODPs of $Sr(Mn_{1-x}W_x)O_3$ are entirely different from that of the fully ordered Sr_2MnWO_6 [25,26,37,38]. Instead of the long-range AFM order [25,26], we found a spin-glass state with transition temperature (T_g) systematically decreasing with x. Such tunability of the site occupancy will be common to nearly all DPs, and hence this approach can prove an interesting way for tailoring the properties of other DPs as well.

II. EXPERIMENT

$Sr(Mn_{1-x}W_x)O_3$ compounds with $x = 0.20$ to 0.40 were prepared following the conventional solid-state reaction route using 99.99% pure $SrCO_3$, MnO_2, and WO_3. The thoroughly ground stoichiometric mixture of the ingredients was calcined and sintered, respectively, at 1200 °C for 24 h and 1450 °C for 12 h. Phase purity characterization was done using powder x-ray diffraction. The charge states of Mn were determined through x-ray photoelectron spectroscopy (XPS) measurements (SPECS, Germany). The magnetization vs temperature (M-T) measurements were carried out under zero-field-cooled (ZFC) and field-cooled (FC) conditions at 500 Oe using SQUID VSM (Superconducting quantum-interference device vibrating sample magnetometer), QD (Quantum design, USA). To investigate the microscopic nature of the magnetic ground states, neutron powder diffraction (NPD) (200–5 K), using the GEM instrument, and muon spin relaxation (μSR) measurements in zero field (ZF) and 0–0.3 T longitudinal fields (LF) (125–2 K), using the MuSR instrument, were performed at the ISIS Pulsed Neutron and Muon Source, UK.

III. RESULTS

A. Neutron diffraction studies

As-prepared samples were subjected to thorough structural characterizations (see Sec. SM 1.0 in the Supplemental Material [40] for details on structural characterization). In the literature, two possible space groups $P4_2/n$ [25] and $P2_1/n$ [26] have been assigned to the structure of $SrMn_{0.5}W_{0.5}O_3$. We refined the room temperature NPD data of all the studied PODPs with $P2_1/n$ using JANA2006 [41]. Figure 1(a) presents typical NPD data (of $x = 0.3$ sample), which have been refined using $P2_1/n$. The refinement of PODP structures was done following coupled $2c$ and $2d$ occupancies described as $Sr_2(Mn_{1-x}W_x)(Mn_yW_{1-y})O_6$ (see Sec. SM 1.3 in the Supplemental Material [40] for details on structure refinement). Figures 1(b) and 1(c) show typical examples of the refined crystal structure of the PODP phase. The relative partial occupancies of Mn($2c$) and W($2d$) sites and the Mn-O-Mn bond angles, along the c axis and in the ab plane, show systematic variation with x; see Table I. It shows that the Mn-O-Mn bond angle along the c axis decreases with increasing x, whereas the second type of Mn-O-Mn bond angle lying in the ab plane remains less affected. The bending of Mn-O-Mn is likely to tilt the anisotropy axis, thereby causing canting of the moments [42,43].

B. Magnetic studies

Temperature-dependent dc magnetic susceptibility (χ_{dc} vs T) of $Sr(Mn_{1-x}W_x)O_3$ was measured for $x = 0.20$ to 0.40. Figures 2(a) and 2(b) show a typical ZFC, and 500 Oe FC χ_{dc} vs T for $x = 0.20$ and 0.30, respectively. The ZFC χ_{dc} vs T shows a sharp cusplike feature at T_g that systematically shifts from 53 to 14 K as x increases from 0.20 to 0.40. The variation of T_g and the corresponding $\chi_{dc}(T_g)$ is shown in Fig. 3. The cusplike feature has also been reported by Lin *et al.* [44] for the fully ordered DP of Sr_2MnWO_6. The ZFC cusp shows bifurcation with the FC curve. The dc susceptibility increases

TABLE I. Refined occupancies, Mn-O-Mn bond angles, and agreement factors. The digits in parentheses represent error (or standard uncertainty) in the last digit of the value.

$SrMn_{1-x}W_xO_3$	GOF			Occupancies		Mn-O-Mn bond angles (deg)	
(x)	(goodness of fit)	R_p	wR_p	Mn ($2c$)	W ($2d$)	Along c axis	In ab plane
0.30	1.03	2.94	3.81	0.404(2)	0.204(2)	177.1758(7)	175.2437(5) and 174.7152(7)
0.32	3.09	3.	4.84	0.406(1)	0.226(1)	170.893(3)	174.9600(9) and 170.9954(7)
0.40	1.86	2.49	3.48	0.474(1)	0.374(1)	161.942(5)	175.6671(8) and 167.704(4)

with (x). To explore the dynamic behavior of the short-range spin correlations, ac susceptibility (χ_{ac} vs T) measurements were carried out at frequencies ranging from 31 to 937 Hz. The χ_{ac} vs T data for $x = 0.2$ and $x = 0.3$ samples are shown in Figs. 2(c) and 2(d). The χ_{ac} vs T data also show a cusplike peak, the frequency dependence of which is shown in the insets of each panel.

To check for the occurrence of any long- or short-range magnetic order, NPD measurements were performed at temperatures below the cusplike anomalies. Figure 4 shows the comparison of the low-q (high-d) regions of the low-temperature NPD profiles of the $Sr(Mn_{1-x}W_x)O_3$ samples with $x = 0.30$, 0.32, and 0.40. In the literature the occurrence of a pronounced AFM peak at ~9.2 Å is reported for $SrMn_{0.5}W_{0.5}O_6$ by Azad *et al.* [25] and Muñoz *et al.* [26], but no such feature is evident in our data, so we conclude the absence of long-range AFM ordering.

C. μSR measurements

To investigate the spin-glass state in the PODP phases of $Sr(Mn_{1-x}W_x)O_3$, low-temperature (125–1.5 K) ZF-μSR measurements were carried out on samples with $x = 0.20$, 0.30, and 0.40 using a 100% spin-polarized pulsed μ^+ beam (duration 70 ns, period 20 ms) at the ISIS facility, UK [45]. The μSR technique probes a much wider time domain, 10^5-10^{10} Hz, of magnetic relaxation than $\chi_{ac}(T)$ [46]. The asymmetry vs time $A(t)$ μSR spectra were collected from 0.1 to 32 μs. The ZF μSR spectra were collected down to 1.5 K; see Sec. SM 3.0 in the Supplemental Material [40] for complete ZF μSR spectra. The $A(t)$ spectra of $Sr(Mn_{1-x}W_x)O_3$ samples with $x = 0.20$, 0.30, and 0.40 show qualitatively similar behavior, except for the lowering of the transition temperature.

In our samples, all Mn ions are magnetic. Since only 20%–40% of these Mn ions are being replaced by W, it is still a relatively dense moment system. After excluding other possible models [47], we analyzed the measured $A(t)$ using a simple exponential and a constant.

$$A(t) = A_r \exp(-\lambda t) + A_c. \quad (1)$$

Here A_r is the amplitude of the relaxing part of the observed asymmetry, λ is the muon spin relaxation rate, and A_c is the constant part of the observed asymmetry, which will have a temperature-independent part from muons stopping outside the sample and a part from muons stopping in the sample but not being depolarized, that may depend on temperature. A_r, A_c, and λ were determined by fitting the $A(t)$ data with Eq. (1) using the MANTID software [48]. At high temperature in the paramagnetic state, $A_r + A_c \sim 0.26$, which is the initial asymmetry expected for the experimental setup.

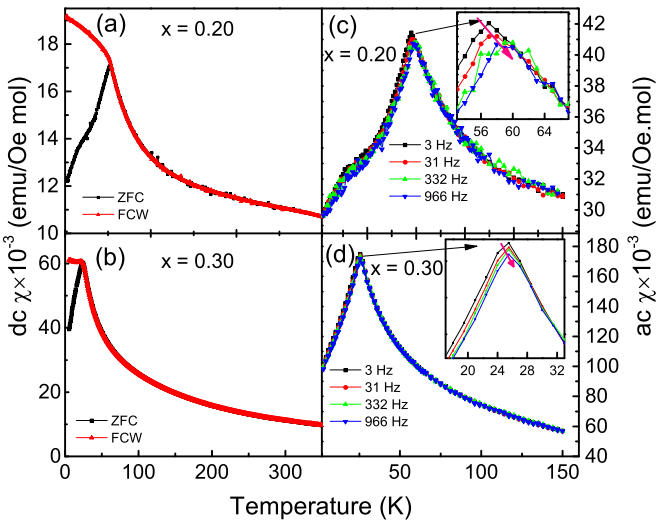

FIG. 2. (a), (b) The temperature variation of $\chi_{dc}(T)$ for $Sr(Mn_{1-x}W_x)O_3$, respectively, for $x = 0.2$ and 0.3. The cusplike peak can be clearly seen. (c), (d) $\chi_{ac}(T)$ variation of $Sr(Mn_{1-x}W_x)O_3$, for $x = 0.20$ and 0.30. Frequency dispersion of the cusplike peaks can be clearly seen in the insets.

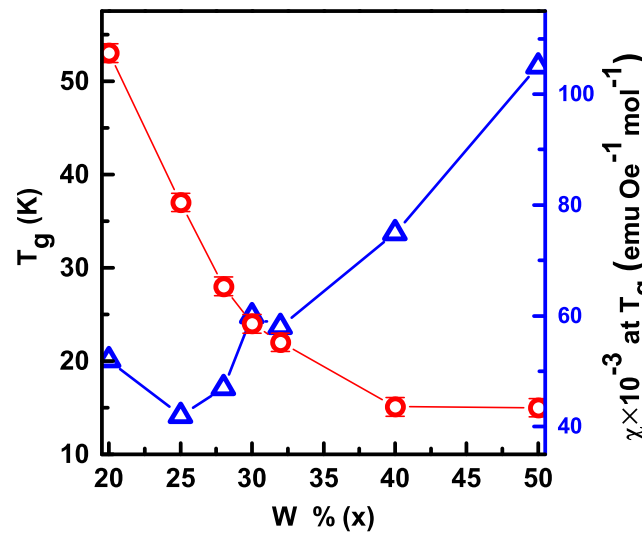

FIG. 3. Variation of spin-glass transition temperature T_g and the $\chi_{dc}(T_g)$, i.e., value of $\chi_{dc}(T)$ at T_g, as a function of W concentration (x). T_g marks the cusp of $\chi_{dc}(T)$.

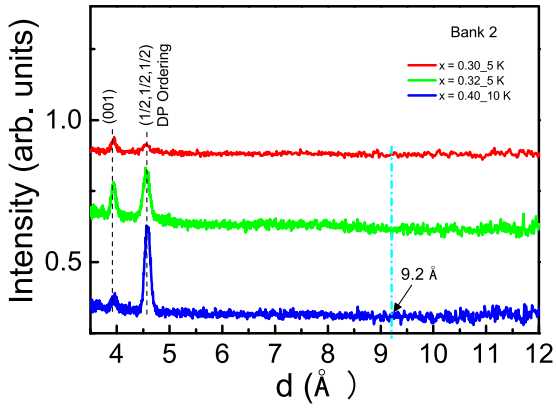

FIG. 4. Enlarged view of the low-q (high-d) regions of the bank-2 TOF-NPD profiles of $Sr(Mn_{1-x}W_x)O_3$ samples with $x = 0.30$, 0.32, and 0.40. Unlike Ref. [26] these profiles clearly depict (dashed vertical line) the absence of any peak at ∼9.2 Å showing AFM order in the PODP phase.

Figures 5(a)–5(f) show the temperature dependence of A_r, A_c, and λ. In each panel of Figs. 5(a)–5(f) the flat behavior of A_r and λ at high temperature shows the paramagnetic state of the samples. As the temperature is lowered across the characteristic temperature (T_g), A_r drops sharply. The steep drop in A_r indicates that the muon spins are depolarized well within the pulse duration of 70 ns. The corresponding cusplike peaks in λ show that the timescale of the fluctuation of the local field is slowing down and crosses the μSR time window of 10 ps to 1 μs, around T_g. Both these anomalies show correspondence with the ac/dc $\chi(T)$ data.

In spin glasses, across the freezing transition, the spin-glass order susceptibility diverges proportional to τ^{-w} [49] where (τ) is the reduced temperature given as $\tau = (T - T_g)/T_g$ and (w) is the critical exponent. When susceptibility diverges, magnetization (i.e., the local field) also diverges and hence the muon spin relaxation rate λ should also diverge [50] as $\lambda = \lambda(0)\tau^{-w}$. In fact the critical exponents measured using μSR have a composite effect of both static and dynamic properties of the moments. Figure 6(a) shows the log(λ) vs $\log\{(T - T_g)/T_g\}$ plots for the three studied samples. The well-defined linear behavior of these plots indicates that λ increases algebraically, i.e., $\lambda = \lambda(0)\tau^{-w}$, as T approaches T_g. The critical growth of $\lambda(T)$ in turn indicates critical slowing down of the spin fluctuations. The complete absence of long-range magnetic order in NPD and the cusplike peak in ac/dc $\chi(T)$ indicate that the slowing down of the spin-fluctuation is due to spin-glass transition at T_g. The value of critical exponents for insulating spin glasses in high reduced temperature is ∼3.3 [46]. However, for the three samples in our case the critical exponents are found to range from 2.09 to 1.04 as (x) increases from $x = 0.20$ to 0.40. This might be due to changes in the degree of isotropy of the exchange interaction [51].

To distinguish between static and fluctuating fields, we collected μSR spectra at 5 K for the $Sr(Mn_{1-x}W_x)O_3$ sample with $x = 0.30$, at various longitudinal fields (LFs) ranging from 0 to 0.3 T. Figure 6(b) shows the corresponding LF $A(t)$ data. Since the applied LFs are unable to decouple the muon spins from the internal local fields they experience, and the form of the data suggests that the fields are quasistatic, we concluded that the internal local fields in the samples are significantly larger than the applied largest longitudinal field of 0.3 T.

IV. DISCUSSION

The bifurcation in ZFC and FC of χ_{dc} vs T below the cusp, the frequency dispersion of the peak maxima in χ_{ac} vs T, the complete absence of the signature of any magnetic order in NPD, and the critical growth of the muon spin relaxation rate $\lambda(T)$, i.e., $\lambda = \lambda(0)r^{-w}$ in ZF μSR studies, clearly reveal that $Sr(Mn_{1-x}W_x)O_3$ with $x = 0.20$ to 0.40 undergoes a spin-glass transition. The significantly low value of magnetization, even at fields as high as 7 T, is due to inherent moment frustration in the spin-glass state. The opening of the M-H loop (see Sec. SM 2.0 in the Supplemental Material [40]) below T_g is due to field irreversibility characteristics of spin glass [15–17] which is seen even in canonical spin-glass systems [52–54].

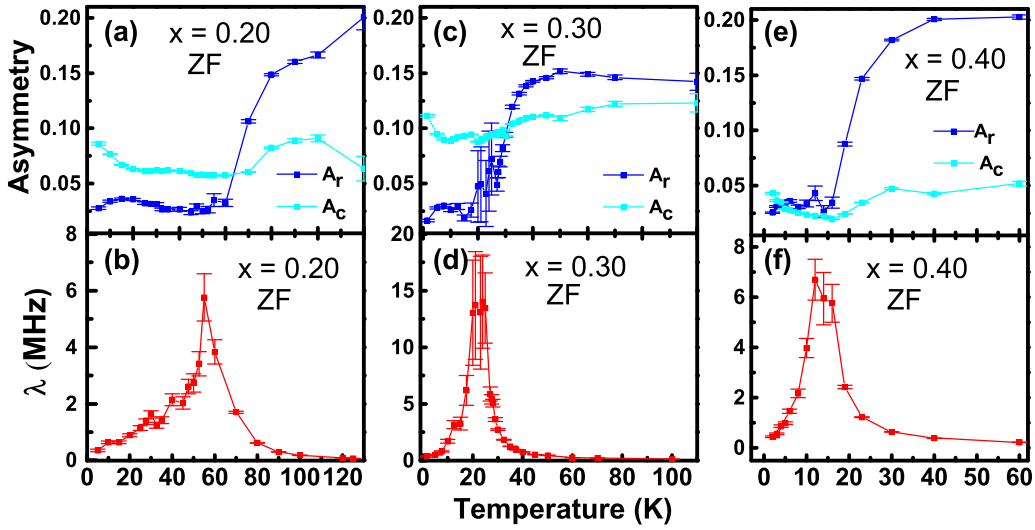

FIG. 5. The temperature variation of A_r, A_c, and λ obtained from the $A(t)$ data. The relaxing asymmetry A_r decreases sharply and λ peaks at T_g.

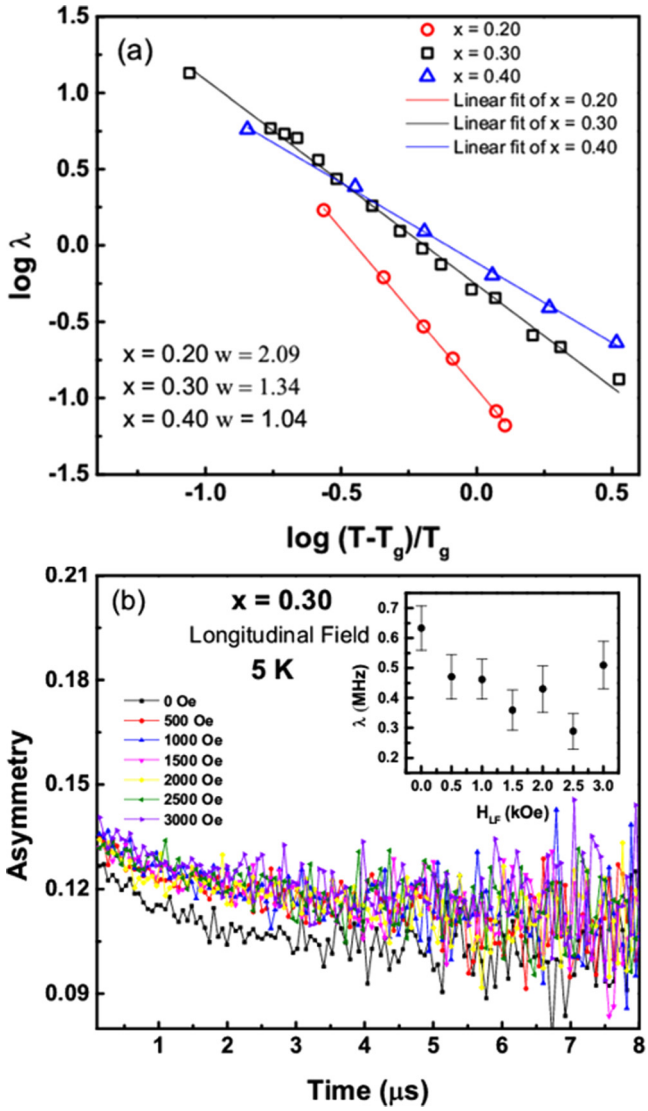

FIG. 6. (a) log(λ) vs log$\{(T-T_g)/T_g\}$ plot showing critical behavior of the spin freezing across the glass transition. Here (w) is the critical exponent of λ. (b) Zero to 0.3 T longitudinal field dependence of $A(t)$ spectra for $x = 0.30$ sample at 5 K.

Upon W doping the effective magnetic moment decreases. A minor increase in the magnetization and the susceptibility, at low temperatures, is due to the weakening of the AFM interaction and a concomitant increase in the ferromagnetic exchange interactions because of charge disorder. The spin-glass transition temperature T_g is supposed to decrease with decreasing the concentration of magnetic ions [55–57]. This is in agreement with our observation.

In pristine $SrMnO_3$, all the Mn ions are in the 4+ charge state. However, in $SrMn_{1-x}W_xO_3$, since the most stable oxidation state of tungsten (W) is 6+, some of the Mn^{4+} convert into Mn^{3+}. The presence of 4+/3+ mixed valence of Mn gives rise to a series of interesting charge and spin ordered states [58] until $x \leqslant 0.18$. As confirmed through XPS measurements (see Sec. SM 4.0 in the Supplemental Material [40]) and its analysis [59–61], in $Sr(Mn_{1-x}W_x)O_3$ with $x \geqslant 0.20$, besides Mn^{4+} and Mn^{3+}, a significant amount of Mn^{2+} is also present, which increases from 23%, to 25%, and 33%, respectively, for $x = 0.20$, 0.25, and 0.30. It is expected that as x approaches 0.5, Mn^{2+} will maximize and concentrations of Mn^{3+} and Mn^{4+} go to zero. Recently, Wang *et al.* [62] have also reported similar changes in the charge state of Mn on W substitution in $Sr(Mn_{1-x}W_x)O_3$. $SrMnO_3$ is a G-type AFM [39] with NN Mn^{4+} t_{2g} moments interacting antiferromagnetically through $Mn^{4+} - O^{2-} - Mn^{4+}$ superexchange pathways. At the other extreme of $x = 0.5$, i.e., in fully ordered DP Sr_2MnWO_6, the Mn^{2+} cations are again ordered antiferromagnetically [25] through $Mn^{2+} - O^{2-} - W^{6+} - O^{2-} - Mn^{2+}$ extended superexchange pathways. However, the intermediate samples with W substitution, e.g., with $x = 0.2$ to 0.4, have mixed charge states Mn^{2+}, Mn^{3+}, and Mn^{4+}, which will cause disordered mixed superexchange interactions leading to magnetic frustration. Some of the possible superexchange models showing antiferro or ferromagnetic interactions between given Mn charge states are shown in Fig. 7(a) (see Sec. 5.0 in the Supplemental Material [40] for details on the GKA rule).

Here, in order to illustrate how magnetic frustration can arise in the lattice of $Sr(Mn_{1-x}W_x)O_3$ having mixed charge states Mn^{2+}, Mn^{3+}, and Mn^{4+}, for simplicity we consider a case of nearly equally populated Mn charge states. Figure 7(b) shows a 2D schematic of the same with B-site cations only. In these compounds both the transition metal ions, viz., Mn and W, are situated in the octahedral crystal field and hence undergo splitting of the otherwise degenerate fivefold d orbitals giving rise to triply degenerate t_{2g} and doubly degenerate e_g levels. The W^{6+} ion with electron configuration $4f^{14}\,5d^{10}$, being diamagnetic, cannot take part in magnetic exchange. Following the Goodenough-Kanamori-Anderson (GKA) rule of superexchange Mn^{2+}, Mn^{3+}, and Mn^{4+} ions with electron configurations $3d^5$, $3d^4$, and $3d^3$, respectively, undergo indirect exchange interaction. The magnetic exchange interactions between Mn^{2+} and Mn^{2+}, Mn^{3+} and Mn^{3+}, and Mn^{4+} and Mn^{4+} are expected to be antiferromagnetic, whereas between Mn^{2+} and Mn^{3+}, Mn^{2+} and Mn^{4+}, and Mn^{3+} and Mn^{4+} it should be ferromagnetic [63]; see Supplemental Material [40]. Magnetic frustration can arise due to (i) geometric constraints (as in triangular or tetrahedral lattices with AFM interaction) or (ii) competing FM and AFM interactions in a lattice. For $SrMn_{1-x}W_xO_3$ compositions with PODP structure, we do not expect any geometric frustration as the underlying tetrahedral topology, on which the magnetic ions are arranged, is distorted due to the $P2_1/n$ space group of the PODP. In the fully disordered case of simple cubic perovskite, the square lattice with AFM interaction is not supposed to cause geometric frustration. On the other hand, the presence of both FM and AFM superexchange interactions, among mixed valence Mn ions, can result in "exchange frustration," particularly when the Mn^{2+}, Mn^{3+}, and Mn^{4+} ions are disordered. The two-dimensional (2D) schematic in Fig. 7(b) shows how competing magnetic interactions between mixed charge states of Mn cations can bring in the exchange frustration in the lattice. When we "start" from a magnetic site, with any randomly selected spin orientation, and navigate through the lattice following the GKA rule, it is found that certain Mn sites cannot simultaneously satisfy exchange interactions with all their neighbors (marked as "?") causing magnetic frustration and thus leading to a spin-glass state. While the 2D

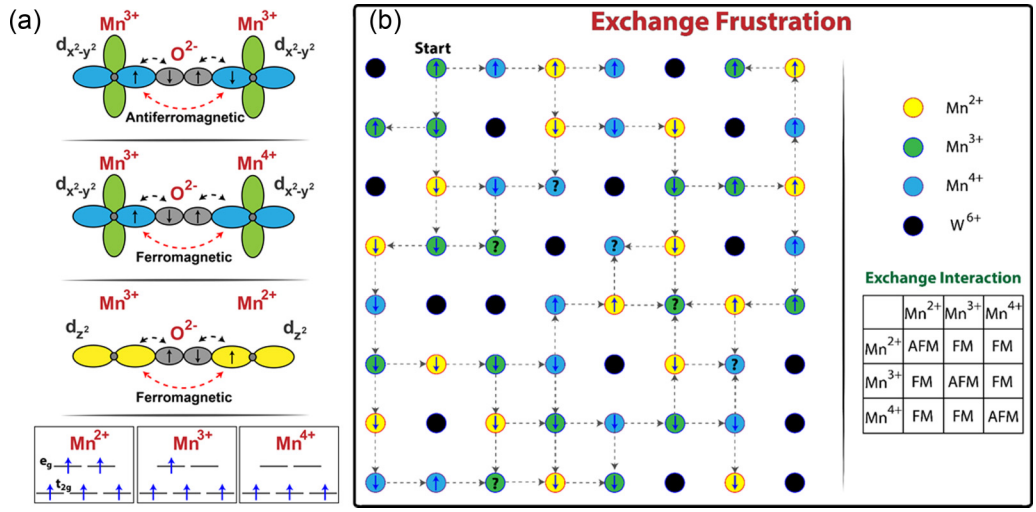

FIG. 7. (a) Some of the possible superexchange models showing antiferro- or ferromagnetic interactions between given Mn charge states. (b) 2D schematic showing proposition of the possible cause of exchange frustration arising due to random distribution of mixed charge states of Mn leading to competing (FM/AFM) superexchange interactios in $Sr(Mn_{1-x}W_x)O_3$, generally expected to occur for samples with $x \geqslant 0.20$.

illustration is somewhat simpler to visualize, the situation becomes extremely complex when we consider visualization in 3D. However, at the same time, allowing interaction paths in three dimensions (3D) enhance the chance of getting more neighbors marked as (?), hence leading to stronger magnetic frustration.

With increasing W, the concentration of Mn^{2+} increases at the expense of Mn^{3+} and Mn^{4+}. Since Mn^{3+} is necessary for charge/orbital order, its decrease suppresses the long-range charge/orbital/spin ordered phases and enhances disordered magnetic phase, leading to spin-glass behavior. The occurrence of Mn^{2+} is thus correlated with the appearance of the spin-glass phase.

Though the above-described model of exchange frustration considers fully disordered Mn charge states distribution, i.e., the limiting case of $x = 0.25$ (see Sec. SM 1.1 in the Supplemental Material [40]), the same argument can be applied for the PODPs as well. Our structural analysis reveals that the PODP phase arises due to partial occupancy of Mn and W, respectively, at $2c$ and $2d$ sites, which changes rather continuously towards $x = 0.5$ for a fully ordered DP. In such an intermediate situation, the fully disordered scenario of Mn charge states is not expected to change much, even if the diffraction data indicate appearance of a PODP phase, e.g., the phases with $0.3 \leqslant x \leqslant 0.4$, and therefore the magnetic frustration will still largely prevail. Of course, the density of Mn sites marked (?) will continuously decrease with increasing (x) and finally the system will slowly terminate to an ordered AFM phase. Like other spin-glass systems [57], the decrease in T_g appears to be related with the decreasing Mn ions in the lattice. In Fig. 8 we summarize the phase diagram of $Sr(Mn_{1-x}W_x)O_3$, showing various magnetic phases as a function of (x) [58].

V. CONCLUSION

Based on the above-described studies on $Sr(Mn_{1-x}W_x)O_3$, with (x) ranging from 0.20 to 0.40, we conclude that on W substitution at Mn site the G-type antiferromagnetic $SrMnO_3$ undergoes a transformation to a disordered simple perovskite dense spin-glass phase at $x \sim 0.20$ and then to partially ordered double perovskite (PODP) spin-glass phases with $x \geqslant 0.3$. The spin-glass transition temperature T_g continuously decreases in the range of 55–15 K with increasing W. In both cases, i.e., simple cubic as well as PODPs, the spin-glass phase appears to arise due to *exchange frustration* between the randomly distributed Mn^{2+}, Mn^{3+}, and Mn^{4+} cations. The spin-glass phase appears to be correlated with the occurrence of Mn^{+2} cations and the onset of competing ferro-antiferro interactions. A magnetic phase diagram has been presented summarizing the occurrence of various magnetic phases as a function of W substitution in $Sr(Mn_{1-x}W_x)O_3$. We finally conclude that under an otherwise favorable *B*-site substitution, a magnetic perovskite phase can continuously transform to a PODP phase with tunability of the related physical properties, e.g., the spin-glass phase in the present study.

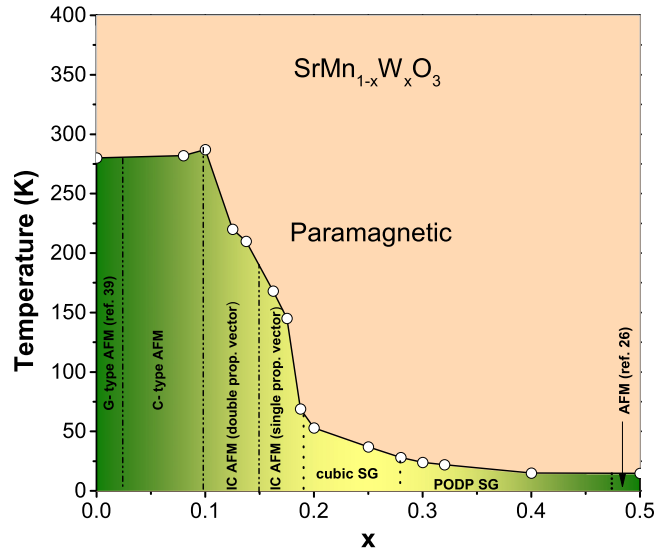

FIG. 8. Phase diagram showing various magnetic phases of $Sr(Mn_{1-x}W_x)O_3$ as a function of (x).

ACKNOWLEDGMENTS

The authors gratefully acknowledge the Director, Dr. A. K. Sinha, and the Centre Director, Dr. V. Ganesan, for their constant support and encouragement. Kranti Kumar is sincerely acknowledged for magnetic measurements. Experiments at the ISIS Neutron and Muon source were supported by a beam time allocation from the Science and Technology Facilities Council (UK).

[1] Y. Shimizu, K. Miyagawa, K. Kanoda, M. Maesato, and G. Saito, Phys. Rev. Lett. **91**, 107001 (2003).

[2] P. Mendels, F. Bert, M. A. de Vries, A. Olariu, A. Harrison, F. Duc, J. C. Trombe, J. S. Lord, A. Amato, and C. Baines, Phys. Rev. Lett. **98**, 077204 (2007).

[3] A. Olariu, P. Mendels, F. Bert, F. Duc, J. C. Trombe, M. A. de Vries, and A. Harrison, Phys. Rev. Lett. **100**, 087202 (2008).

[4] L. Balents, Nature **464**, 199 (2010).

[5] T.-H. Han, J. S. Helton, S. Chu, D. G. Nocera, J. A. Rodriguez-Rivera, C. Broholm, and Y. S. Lee, Nature **492**, 406 (2012).

[6] M. A. de Vries, A. C. Mclaughlin, and J.-W. G. Bos, Phys. Rev. Lett. **104**, 177202 (2010).

[7] J. A. Mydosh, J. Magn. Magn. Mater. **7**, 237 (1978).

[8] C. A. M. Mulder, A. J. van Duyneveldt, and J. A. Mydosh, Phys. Rev. B **23**, 1384 (1981).

[9] J. A. Mydosh, in *20th Annual Conference on Magnetism and Magnetic Materials, San Francisco, 1974*, edited by C. D. Graham, Jr., G. H. Lander, and J. J. Rhyne, AIP Conf. Proc. No. 24 (AIP, New York, 1975), p. 131.

[10] Y. J. Uemura, D. R. Harshman, M. Senba, E. J. Ansaldo, and A. P. Murani, Phys. Rev. B **30**, 1606(R) (1984).

[11] Y. J. Uemura, T. Yamazaki, D. R. Harshman, M. Senba, and E. J. Ansaldo, Phys. Rev. B **31**, 546 (1985).

[12] S. T. Bramwell, Science **294**, 1495 (2001).

[13] H. Kadowaki, Y. Ishii, K. Matsuhira, and Y. Hinatsu, Phys. Rev. B **65**, 144421 (2002).

[14] P. W. Anderson, Mater. Res. Bull. **8**, 153 (1973).

[15] K. Binder and A. P. Young, Rev. Mod. Phys. **58**, 801 (1986).

[16] K. H. Fischer and J. A. Hertz, *Spin Glasses* (Cambridge University Press, Cambridge, 1991).

[17] J. A. Mydosh, *Spin Glasses: An Experimental Introduction* (Taylor and Francis, London, 1993).

[18] *Frustrated Spin Systems*, edited by H. T. Diep (World Scientific, Singapore, 2004).

[19] I. Syôzi, Prog. Theor. Phys. **6**, 306 (1951).

[20] B. S. Shastry and B. Sutherland, Phys. B (Amsterdam, Neth.) **108**, 1069 (1981).

[21] C. R. Wiebe, J. E. Greedan, G. M. Luke, and J. S. Gardner, Phys. Rev. B **65**, 144413 (2002).

[22] T. Aharen, J. E. Greedan, C. A. Bridges, A. A. Aczel, J. Rodriguez, G. MacDougall, G. M. Luke, V. K. Michaelis, S. Kroeker, C. R. Wiebe, H. Zhou, and L. M. D. Cranswick, Phys. Rev. B **81**, 064436 (2010).

[23] C. R. Wiebe, J. E. Greedan, P. P. Kyriakou, G. M. Luke, J. S. Gardner, A. Fukaya, I. M. Gat-Malureanu, P. L. Russo, A. T. Savici, and Y. J. Uemura, Phys. Rev. B **68**, 134410 (2003).

[24] M. T. Anderson, K. B. Greenwood, G. A. Taylor, and K. R. Poeppelmeier, Prog. Solid State Chem. **22**, 197 (1993).

[25] A. K. Azad, S. A. Ivanov, S. G. Eriksson, J. E. Eriksen, H. Rundlöf, R. Mathiew, and P. Svedlindh, J. Magn. Magn. Mater. **237**, 124 (2001).

[26] A. Muñoz, J. A. Alonso, M. T. Casais, M. J. Martinez-Lope, and M. T. Fernandez-Diaz, J. Phys.: Condens. Matter **14**, 8817 (2002).

[27] D. Serrate, J. M. De Teresaand, and M. R. Ibarra, J. Phys.: Condens. Matter **19**, 023201 (2007).

[28] R. Morrow, J. Yan, M. A. McGuire, J. W. Freeland, D. Haskel, and P. M. Woodward, Phys. Rev. B **92**, 094435 (2015).

[29] T. S. Chan, R. S. Liu, G. Y. Guo, S. F. Hu, J. G. Lin, J. M. Chen, and C. R. Chang, Solid State Commun. **133**, 265 (2005).

[30] H.-T. Jeng and G. Y. Guo, Phys. Rev. B **67**, 094438 (2003).

[31] P. D. Battle, J. B. Goodenough, and R. Price, J. Solid State Chem. **46**, 234 (1983).

[32] P. D. Battle and W. J. Macklin, J. Solid State Chem. **52**, 138 (1984).

[33] P. D. Battle and C. W. Jones, J. Solid State Chem. **78**, 108 (1989).

[34] P. D. Battle, C. P. Grey, M. Hervieu, C. Martin, C. A. Moore, and Y. Paik, J. Solid State Chem. **175**, 20 (2003).

[35] L. Ortega-San Martin, J. P. Chapman, L. Lezama, J. J. S. Garitaonandia, J. S. Marcos, J. Rodriguez-Fernandez, M. I. Arriortua, and T. Rojo, J. Mater. Chem. **16**, 66 (2006).

[36] A. K. Azada, S. A. Ivanov, S.-G. Erikssona, J. Eriksen, H. Rundlof, R. Mathieu, and P. Svedlindh, Mater. Res. Bull. **36**, 2215 (2001).

[37] C. P. Khattak, D. E. Cox, and F. F. Y. Wang, J. Solid State Chem. **17**, 323 (1976).

[38] J.-W. G. Bos and J. P. Attfield, Phys. Rev. B **70**, 174434 (2004).

[39] T. Takeda and S. Ohera, J. Phys. Soc. Jpn. **37**, 275 (1974).

[40] See Supplemental Material at http://link.aps.org/supplemental/10.1103/PhysRevB.99.214421 for additional details/information on structural, magnetic, μSR, and XPS characterizations and superexchange interaction.

[41] V. Petříček, M. Dušek, and L. Palatinus, Z. Kristallogr. **229**, 345 (2014).

[42] I. Dzyaloshinskii, J. Phys. Chem. Solids **4**, 241 (1958).

[43] T. Moriya, Phys. Rev. **120**, 91 (1960).

[44] Q. Lin, M. Greenblatt, and M. Craft, J. Solid State Chem. **178**, 1356 (2005).

[45] A. D. Hillier, D. J. Adams, P. J. Baker, A. Bekasovs, F. C. Coomer, S. P. Cottrell, S. D. Higgins, S. J. S.Jago, K. G. Jones, J. S. Lord, A. Markvardsen, P. G. Parker, J. N. T. Peck, F. L. Pratt, M. T. F. Telling, and R. E. Williamson, J. Phys.: Conf. Ser. **551**, 012067 (2014).

[46] L. Nuccio, L. Schulz, and A. J. Drew, J. Phys. D: Appl. Phys. **47**, 473001 (2014).

[47] R. S. Hayano, Y. J. Uemura, J. Imazato, N. Nishida, T. Yamazaki, and R. Kubo, Phys. Rev. B **20**, 850 (1979).

[48] MANTID (2013): Manipulation and analysis toolkit for instrument data: MANTID project; http://dx.doi.org/10.5286/SOFTWARE/MANTID.

[49] H. Bouchiat, N. de Courtenay, and P. Monod, Jpn. J. Appl. Phys. **26**, 1951 (1987).
[50] M. Attenborough, I. Hall, O. Nikolov, S. R. Brown, and S. F. J. Cox, Hyperfine Interact. **108**, 423 (1997).
[51] H. Kawamura, J. Phys.: Conf. Ser. **233**, 012012 (2010).
[52] P. A. Beck, Prog. Mater. Sci. **23**, 1 (1978).
[53] P. Monod, J. J. Prejean, and B. Tissier, J. Appl. Phys. **50**, 7324 (1979).
[54] J. J. Prejean, M. Joliclerc, and P. Monod, J. Phys. (Paris) **41**, 427 (1980).
[55] D. C. Vier and S. Schultz, Phys. Rev. Lett. **54**, 150 (1985).
[56] M. R. A. Shegelski and D. J. W.Geldart, Phys. Rev. B **46**, 2853 (1992).
[57] H. Bednarski and J. Cisowski, Acta Phys. Pol., A **82**, 868 (1992).
[58] We have studied SrMnWO compositions ranging from $x = 0.08$ to 0.40. In the present report we are giving the results of compositions $x = 0.2$ to 0.4 only. The lower compositions show incommensurate charge and AFM ordering. The results of lower W composition will be reported soon in a separate publication.
[59] M. A. Stranick, Surf. Sci. Spectra **6**, 39 (1999).
[60] M. A. Stranick, Sur. Sci. Spectra **6**, 31 (1999).
[61] V. Di Castro and G. Polzonetti, J. Electron. Spectrosc. Relat. Phenom. **48**, 117 (1989).
[62] J.F. Wang, V. M. Zhang, C. Jie, and M. Xu, J. Phys. D: Appl. Phys. **50**, 305001 (2017).
[63] J. B. Goodenough, Phys. Rev. **100**, 564 (1955).